Radioluminescence properties of decaoctahedral BaZrO3

ARTICLE *in* SCRIPTA MATERIALIA · SEPTEMBER 2011

Impact Factor: 3.22 · DOI: 10.1016/j.scriptamat.2010.09.017

Available online at www.sciencedirect.com
ScienceDirect
Scripta Materialia 64 (2011) 118–121
Scripta MATERIALIA
www.elsevier.com/locate/scriptamat

Radioluminescence properties of decaoctahedral $BaZrO_3$

Mário L. Moreira,[a,*] Diogo P. Volanti,[a] Juan Andrés,[b] Paulo J.R. Montes,[c] Mário E.G. Valerio,[c] José A. Varela[a] and Elson Longo[a]

[a] *INCTMN, Physical Chemistry Department, Institute of Chemistry, Unesp, Araraquara, SP 14800-900, Brazil*
[b] *Departament de Química Física i Analítica, Universitat Jaume I, Campus de Riu Sec, Castelló E-12080, Spain*
[c] *INCT-INAMI, Physics Department, Federal University of Sergipe, São Cristóvão, Sergipe 49100-000, Brazil*

Received 2 September 2010; accepted 13 September 2010
Available online 17 September 2010

Radioluminescence (RL) emissions were obtained for the $BaZrO_3$ self-assembled nanocrystals under decaoctahedral shape, if produced via microwave-assisted hydrothermal method. Trapped *F* centers created within the band gap are the result of order–disorder effects, which act as key factors supporting significant RL emission through a detrapping process. The influences of size and morphology on RL properties are take into account. No radiation damage or loss of emission intensity was observed.

Keywords: Luminescence; Perovskite; Scintillator; Self-assemble; Microwave-assisted hydrothermal method

The study of optical properties in perovskite structures can shed light on the key role played by defects/impurities and other order–disorder effects that are related to their potential applications [1,2]. Materials that convert ionizing radiation, such as X-rays, α-, β- and γ-rays, or UV incident beams into visible or IR light (scintillators) have attracted special attention [3]. A good scintillator has to exhibit high quantum efficiency in converting the absorbed energy into visible photon emissions [4]. Other desirable characteristics are chemical and physical stability, a high radiation damage threshold and a time response compatible with the desired application [4]. In recent years, several researches have demonstrated the growing potential of pure scintillator materials and/or those doped with rare earth elements [5,6]]. To understand the phenomena involved in the process of radioluminescence (RL) emission, Nikl [3] proposed a general model that can be extended to other compounds.

$BaZrO_3$ (BZO) perovskite presents an appropriate electronic structure and has excellent properties due to a high dielectric constant and a reasonable wide band gap of ~5.4 eV [7]. A variety of methodologies have been reported to produce different sizes and shapes of BZO with refined control on the morphology [4,8].

The exploration of novel synthetic methodologies to control both size and shape opens new avenues for the functional application of such materials. Komarneni et al. [9,10] introduced the microwave-assisted hydrothermal (MAH) method for the synthesis of several electro-ceramics. Bilecka and Niederberger [11] also published an overview of microwave-assisted liquid-phase routes to inorganic nanomaterials. Recently, Strauss et al. [12] published a critical review, emphasizing clean, fast and high-yielding reactions under microwave conditions.

The MAH method can also be considered as a green and sustainable method for the self-assembly of metal oxides into three-dimensional nanostructures [9,13]. Microwave irradiation is also unique in providing scaled-up processes without suffering from thermal gradient effects, thus opening up new avenues for the potential production of high-quality nanomaterials [14–16]. Our group has expanded various efforts to demonstrate that the MAH method is one of most versatile and highly cost-effective approaches to obtain crystalline, micro- and/or nanoscale materials [17–19].

For purposes of comparison, we first prepared a reference BZO sample (BZOref) by the Pechini method (PM) heat treated at 700 °C for 2 h in air using a typical muffle. BZO powders prepared by the MAH method were reported in detail by Moreira et al. [17] (see Supplementary material) being that BZO10 correspond to 10 min of synthesis and so on. The samples were characterized by X-ray diffraction by adsorption–desorption

* Corresponding author. Tel./fax: +55 16 3351 8214; e-mail: mlucio@liec.ufscar.br

1359-6462/$ - see front matter © 2010 Acta Materialia Inc. Published by Elsevier Ltd. All rights reserved.
doi:10.1016/j.scriptamat.2010.09.017

isotherms of N2, FE-SEM microscopy and optical absorption coefficients using Varian Cary 5G spectrometer. The RL spectra were recorded under X-ray excitation (Cu K_α) using an Ocean Optics HR2000 spectrometer equipped with an optical fiber.

The main structural properties, crystalline phases, morphology, surface areas, average size of particle, lattice parameter, density and optical band gap of BZO powders are listed in Table 1, while the RL emissions of BZO synthesized via the MAH and PM at room temperature are presented in Figure 1. The constituent phases for each synthesis time could be identified from the XRD powder patterns (see Fig. 2). After 20 min, all samples show a cubic structure with a small amount of a $BaCO_3$ phase. The cubic structure is preferable for ceramic scintillators to prevent scattering and to avoid differences in the refractive index of the lattice directions [20]. A continuous evolution of the cubic BZO phase formation is evidenced by the main (1 1 0) diffraction, which is related to the periodic arrangement of both cube–octahedral (BaO_{12}) and octahedral (ZrO_6) clusters [17] (see Fig. 2). The surface area decreases from 156 to 39 $m^2\ g^{-1}$ with increasing synthesis time. Moreover, a high porosity may be easily detected by an analysis of the images displayed in Figure 2. The decaoctahedral shape is an important factor, as was pointed out by Wang [21] regarding the network tensions mechanism. As the tension increases, the morphology of the self-assembled nanocrystals changes from a quasi-spherical to a decaoctahedral shape (see Fig. 2c–e) [17]. This architecture has attracted much attention because it exhibits unique optical properties which are dependent not only on size but also the shape [17,22]. Similarly, samples BZO40 up to BZO160 show an abrupt reduction in area, indicating that these particles have propensity to form more homogeneous crystals by the densification process as a result of porous elimination.

In particular, the presence of distorted octahedrons and cube–octahedrons has been employed to understand the origin of the photoluminescence (PL) behavior of BZO with a crystalline and disordered structure obtained by the PM [23] not flaunting any RL emission, as reported in Figure 1. Disorder features can be enhanced by the inherently high reaction rates, direct interaction of radiation with the matter and the participation of reminiscent OH groups like impurities in the crystallization process.

Optical direct allowed band gaps (E_g) of BZO crystals were obtained from UV–visible absorbencies using Wood and Tauc approach [24], which are listed in Table 1 [17]. Our BZO samples are capable of converting ionizing radiation into visible light emission at the blue-green region of solar spectra as shown in Figure 1. The RL visible emission becomes more defined and intense as the more ordered BZO phase is achieved in accordance to the E_g evolution (Table 1). Also, during the RL recording no apparent radiation damage was observed for exposure times of till 50 s, thus the quantum efficiency scintillation of BZO is preserved [25]. A second group of emission bands around 600–700 nm does not display an apparent dependence on structural changes.

The RL process can be rationalized in a series of consecutive stages, as shown in the schematic model of Figure 3. In the first stage, X-ray high-energy absorption

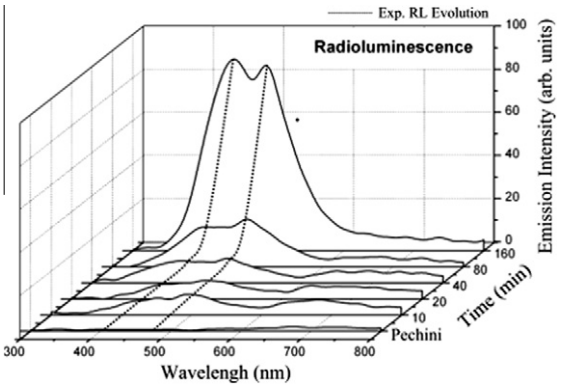

Figure 1. RL emissions for BZO samples synthesized by the Pechini and MAH methods.

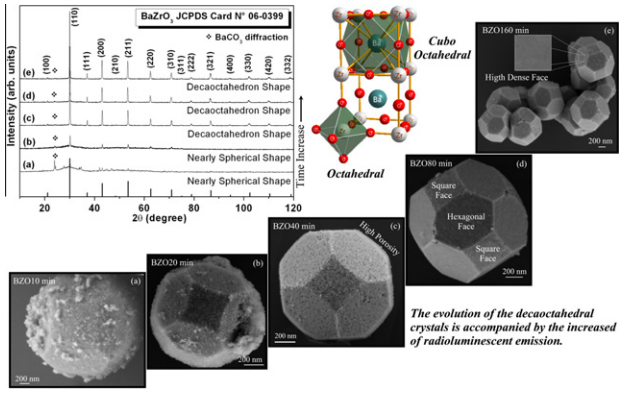

Figure 2. Powder XRD patterns and FE-SEM microscopy of BZO decaoctahedrons obtained via the MAH method at 413 K for (a) 10, (b) 20, (c) 40, (d) 80 and (e) 160 min. A schematic double unit cell with octahedral and cube–octahedral clusters is depicted.

Table 1. Structural, morphological and optical characteristics of BZO samples obtained by MAH.

Sample	Time (min)	Phase	Morphology	Band gap (eV)	Surface area ($m^2\ g^{-1}$)	Lattice parameter $a = b = c$ (Å)	Density ($g\ cm^{-3}$)	Particle size (μm)
BZO10	10	$BaZrO_3$[a]/$BaCO_3$[b]	Nearly spherical	4.78	156.7	Not analyzed	Not analyzed	2.7 ± 0.2
BZO20	20	$BaZrO_3$[a]/$BaCO_3$[b]	Nearly spherical	4.89	156.6	Not analyzed	Not analyzed	2.5 ± 0.3
BZO40	40	$BaZrO_3$[a]/$BaCO_3$[b]	Decaoctahedron	4.98	47.7	4.2115	6.147	2.5 ± 0.4
BZO80	80	$BaZrO_3$[a]/$BaCO_3$[b]	Decaoctahedron	4.99	48.3	4.2081	6.162	2.2 ± 0.3
BZO160	160	$BaZrO_3$[a]/$BaCO_3$[b]	Decaoctahedron	4.99	39.3	4.2062	6.171	1.9 ± 0.1

[a] Cubic (*Pm3m*).
[b] Orthorhombic (*Pmcn*).

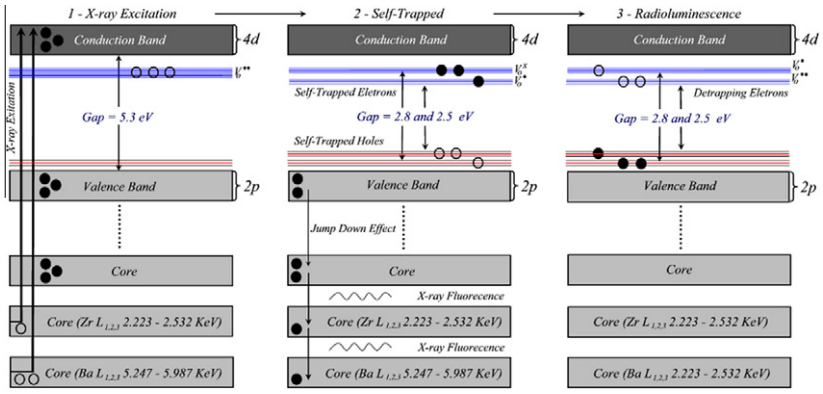

Figure 3. Schematic representation of the radioluminescence excitation and emission mechanisms. The process can be divided into three consecutive steps: conversion (absorption), recombination (trapping) and radioluminescence.

occurs via photoelectron processes via absorption of the incident photons by the Ba and Zr ions. The two main X-ray fluorescence K_α lines of Cu are around 8 keV, a value three orders of magnitude higher than the E_g of BZO. The K-edge absorption values of Zr and Ba are around 18 and 37.5 keV, respectively, which are much higher than the incident photon energy. However, the $L_{1,2,3}$ absorption edges of Zr are between 2.2 and 2.6 keV, while the $L_{1,2,3}$ absorption edges of Ba are in the range from 5.2 to 6 keV. Thus, the primary interaction of the X-ray photons would be via a photoelectric effect removing the electrons of the Ba L shell, which generates a great number of electron–hole pairs. The Ba L shell is rapidly filled by the decay of M and N electrons and thus generates secondary L_α and L_β X-ray fluorescence. The L_α and L_β Ba photon energies are within the 4.4–4.9 keV range. These photons can now interact with the Zr, releasing the $L_{1,2,3}$ electrons and generating a cascade of electron–hole pairs (see Fig. 3) and X-ray photons within the matrix until all the energy of the incident beam is absorbed in the matrix. Alternatively, the incident beam can be absorbed directly by the Zr, also releasing the $L_{1,2,3}$ electrons. In both cases, the consequence will be the same: a full cascade of recombination of electrons from higher shells, ending with a large number of electrons and holes in the conduction (CB) and valence (VB) bands, respectively.

The second stage involves the thermalization of the electron–hole pairs in the CB and VB, respectively, until the electrons reach the bottom of the CB and the holes reach the top of the VB. Two different routes are possible from here. Either the electrons and holes recombine, emitting photons with energy close to the band gap, or the electrons and holes can be trapped at defects that already exist in the band gap. The direct recombination of the charge carriers will give rise to an RL emission with photons in range of 4.8–5.3 eV, equivalent to 245–260 nm, which is not the case observed in our BZO samples. Incidentally, Blasse and Grabmaier [26] verified that the radiative emission process occurs more easily if trapped holes and/or electrons exist in the band gap structure.

There are a number of possible candidates for electron- or hole-trapping centers. The most obvious traps for electrons are anion vacancies, and this seems to be the case for BZO since oxygen vacancies have already been identified in this disordered material, with PL emissions [23] producing lattice polarizations, which are also caused by activation of Raman modes in cubic structures [17]. Cavalcante et al. [23] showed that the electron paramagnetic resonance signal with $g = 2.00038$ could be impute to $V_O^\bullet$, i.e. an oxygen vacancy that trapped an electron, forming an F^- type center. There is also a chance that a second electron can be trapped in such defect, thus forming V_O, which is a neutral F center; for the hole traps, Ba vacancies are the best candidates. These have a significant effect on the low-frequency Ba–O bond, changing the dielectric constant as a result of the density of states redistributions [27], as suggested previously for the PL interrelated with Raman results [17]. This phenomenon is expected to trigger significant electronic charge redistributions, such as the flow of electrons through adjacent $[ZrO_6]$ and $[BaO_{12}]$ clusters.

Moreover, a small amount of $BaCO_3$ was found, meaning that the final $BaZrO_3$ phase had a deficiency of Ba atom. Furthermore, no significant amount of chloride ions was detected, in contrast to what was reported by Clearfield and Vaughan [28,29] (see Support information). We hold that, in our case, the microwave radiation is probably the main reason for this decrease owing to the ionic conduction promoted by the coupling of the electromagnetic field and clusters in solution. Incidentally, the rapid dehydration is related to the same kind of interactions, although in this case producing molecular rotation to improve the dehydration process.

After trapping electrons, the $V_O^{\bullet\bullet}$ energy levels are expected to change their depth from the CB, depending on whether they were filled with one or two electrons. The neutral F type center is expect to be shallower in the forbidden gap than the F^- defect since the energy to remove an electron from the trap to the conduction band will be lower for the F center than for the F^- center, generating intra-gap levels with different energies. Another possible contribution to the formation of F centers is the OH groups in the crystal lattice of the BZO [30], as was observed previously [31,32].

The last stage involves the recombination of the charge carriers, via RL emission, re-establishing the initial conditions of the sample. Considering that the charge carriers are trapped, four main routes can generate the RL emissions: (i) detrapping of the electrons and their recombination with trapped holes; (ii) detrapping

of the holes and their recombination with trapped electrons; (iii) detrapping of the electrons and holes and direct intraband recombination; or (iv) recombination of the trapped electrons with the trapped holes via a tunneling. Processes (i)–(iii) are normally delayed because the trapped charge has to be released from the traps before any recombination takes place. The time delay between the creation of the trapped charge and the actual recombination and emission processes depends greatly on the depth of the trap and the sample temperature.

The final stage consists of the consecutive electron–hole radiative recombination to yield the RL emission ($h\nu'$) in the visible range. Both the presence as well population of the interband states play key roles, and are responsible for the RL emissions. When a highly ordered state is reached (BZO160), two well-defined maxima are presented at 443 nm (~2.8 eV) for a component of blue emission and 490 nm (~2.5 eV) for a component of blue-green emission. These emissions can be associated with various energy states within the band gap created by the redistribution of electronic density resulting from oxygen vacancies $V_O^{\bullet\bullet}$ and $V_O^{\bullet}$. Furthermore, the increase in RL emission for BZO160 is related to its greater stopping power, owing to its more dense surfaces, as denoted by Figure 2e. In this context, it is important to note that this behavior is similar to the PL phenomena found in related materials [23,33,34]. Note that the normal excitation energy of PL is of the order of 2.5–3.5 eV, while the X-ray irradiation is around to 8 keV. Any attempt to obtain BZO samples with RL properties by several methods has been unsuccessful to date. Thus the RL phenomenon is strongly synthetic-method-dependent.

Here, we report a new and versatile approach to synthesize BZO RL self-assembled nanocrystals. The morphologies can be controlled to a great extent by the MAH conditions. The presence of order–disorder effects, like cation and anion vacancies, in the structure of the material can create trapped *F* centers for electrons and holes, which are the key factors promoting the conversion of ionizing radiation into visible light RL emission through a detrapping process of electron and holes. Our results suggest that the MAH method may be an innovative approach for synthesizing other compounds presenting RL properties, and could enhance their intrinsic features for use in existing applications, attracting more attention to this fascinating area of research.

Thanks to CNPq, FAPESP, national institutions INCTMN and INCT-INAMI. Acknowledges to Ministerio de Educación y Cultura of the Spanish Government.

Supplementary data associated with this article can be found, in the online version, at doi:10.1016/j.scriptamat.2010.09.017.

[1] P.K. Davies, H. Wu, A.Y. Borisevich, I.E. Molodetsky, L. Farber, Annu. Rev. Mater. Res. 38 (2008) 369–401.
[2] S. Stolen, E. Bakken, C.E. Mohn, Phys. Chem. Chem. Phys. 8 (2006) 429–447.
[3] M. Nikl, Meas. Sci. Technol. 17 (2006) R37–R54.
[4] G. Blasse, Chem. Mater. 6 (1994) 1465–1475.
[5] K.W. Kramer, P. Dorenbos, H.U. Gudel, C.W.E.v. Eijk, J. Mater. Chem. 16 (2006) 2773–2780.
[6] C. Mansuy, J.-M. Nedelec, R. Mahiou, J. Mater. Chem. 14 (2004) 3274–3280.
[7] G. Lupina, J. Dabrowski, P. Dudek, G. Kozlowski, P. Zaumseil, G. Lippert, O. Fursenko, J. Bauer, C. Baristiran, I. Costina, H.J. Muuessig, L. Oberbeck, U. Schroder, Appl. Phys. Lett. 94 (2009) 152903-1–152903-3.
[8] V. Polshettiwar, B. Baruwati, R.S. Varma, ACS Nano 3 (2009) 728–736.
[9] S. Komarneni, Q. Li, K.M. Stefansson, R. Roy, J. Mater. Res. 8 (1993) 3176–3183.
[10] S. Komarneni, R. Roy, Q.H. Li, Mater. Res. Bull. 27 (1992) 1393–1405.
[11] I. Bilecka, M. Niederberger, Nanoscale 2 (2010) 1358–1374.
[12] C.R. Strauss, D.W. Rooney, Green Chem. 12 (2010) 1340–1344.
[13] M. Niederberger, H. Colfen, Phys. Chem. Chem. Phys. 8 (2006) 3271–3287.
[14] I. Bilecka, I. Djerdj, M. Niederberger, Chem. Commun. (2008) 886–888.
[15] Q.Y. Lu, F. Gao, S. Komarneni, J. Mater. Res. 19 (2004) 1649–1655.
[16] S. Makhluf, R. Dror, Y. Nitzan, Y. Abramovich, R. Jelinek, A. Gedanken, Adv. Funct. Mater. 15 (2005) 1708–1715.
[17] M.L. Moreira, J. Andres, J.A. Varela, E. Longo, Cryst. Growth Des. 9 (2009) 833–839.
[18] M.L. Moreira, E.C. Paris, G.S. do Nascimento, V.M. Longo, J.R. Sambrano, V.R. Mastelaro, M.I.B. Bernardi, J. Andres, J.A. Varela, E. Longo, Acta Mater. 57 (2009) 5174–5185.
[19] A.E. Souza, R.A. Silva, G.T.A. Santos, M.L. Moreira, D.P. Volanti, S.R. Teixeira, E. Longo, Chem. Phys. Lett. 488 (2010) 54–56.
[20] C. Ronda, Luminescence: From Theory to Applications, Wiley-VCH, Weinheim, 2008.
[21] Z.L. Wang, J. Phys. Chem. B 104 (2000) 1153–1175.
[22] J.J. Urban, J.E. Spanier, O.Y. Lian, W.S. Yun, H. Park, Adv. Mater. 15 (2003) 423–426.
[23] L.S. Cavalcante, V.M. Longo, M. Zampieri, J.W.M. Espinosa, P.S. Pizani, J.R. Sambrano, J.A. Varela, E. Longo, M.L. Simoes, C.A. Paskocimas, J. Appl. Phys. 103 (2008) 8.
[24] D.L. Wood, J. Tauc, Phys. Rev. B 5 (1972) 3144–3151.
[25] P.J.R. Montes, M.E.G. Valerio, G.D. Azevedo, Nucl. Instrum. Methods Phys. Res. Sect. B 266 (2008) 2923–2927.
[26] G. Blasse, B.C. Grabmaier, Luminescent Materials, Springer-Verlag, Berlin, 1994.
[27] J.W. Bennett, I. Grinberg, A.M. Rappe, Phys. Rev. B 73 (2006) 1–4.
[28] A. Clearfield, Rev. Pure Appl. Chem. 14 (1964) 91–94.
[29] A. Clearfield, P.A. Vaughan, Acta Crystallogr. 9 (1956) 555–558.
[30] T. Omata, M. Takagi, S. Otsuka-YAO-Matsuo, Solid State Ionics 168 (2004) 99–109.
[31] W. Munch, K.D. Kreuer, G. Seifertli, J. Majer, Solid State Ionics 125 (1999) 39–45.
[32] Y. Shiratori, C. Pithan, J. Dornseiffer, R. Waser, J. Raman Spectrosc. 38 (2007) 1288–1299.
[33] E. Orhan, F.M. Pontes, M.A. Santos, E.R. Leite, A. Beltran, J. Andres, T.M. Boschi, P.S. Pizani, J.A. Varela, C.A. Taft, E. Longo, J. Phys. Chem. B 108 (2004) 9221–9227.
[34] D.P. Volanti, I.L.V. Rosa, E.C. Paris, C.A. Paskocimas, P.S. Pizani, J.A. Varela, E. Longo, Opt. Mater. 31 (2009) 995–999.